NANO LETTERS

Letter

pubs.acs.org/NanoLett

All-Optical Sensing of a Single-Molecule Electron Spin

A. O. Sushkov,[†,‡,¶] N. Chisholm,[§,¶] I. Lovchinsky,[†,¶] M. Kubo,[‡] P. K. Lo,[∥] S. D. Bennett,[†] D. Hunger,[⊥] A. Akimov,[#] R. L. Walsworth,[†,▽,○] H. Park,*[,†,‡,◆] and M. D. Lukin*[,†]

[†]Department of Physics, [‡]Department of Chemistry and Chemical Biology, [§]School of Engineering and Applied Sciences, Harvard University, Cambridge, Massachusetts 02138, United States

[∥]Department of Biology and Chemistry, City University of Hong Kong, Tat Chee Avenue, Kowloon, Hong Kong SAR, China

[⊥]Max-Planck-Institut für Quantenoptik, Garching D-85748, Germany

[#]Russian Quantum Center, Skolkovo, Moscow Region 143025, Russia

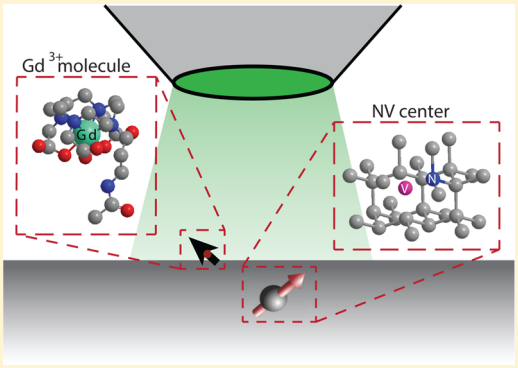
[▽]Harvard-Smithsonian Center for Astrophysics, Cambridge, Massachusetts 02138, United States

[○]Center for Brain Science, Harvard University, Cambridge, Massachusetts 02138, United States

[◆]Broad Institute of MIT and Harvard, 7 Cambridge Center, Cambridge, Massachusetts 02142, United States

Supporting Information

ABSTRACT: We demonstrate an all-optical method for magnetic sensing of individual molecules in ambient conditions at room temperature. Our approach is based on shallow nitrogen-vacancy (NV) centers near the surface of a diamond crystal, which we use to detect single paramagnetic molecules covalently attached to the diamond surface. The manipulation and readout of the NV centers is all-optical and provides a sensitive probe of the magnetic field fluctuations stemming from the dynamics of the electronic spins of the attached molecules. As a specific example, we demonstrate detection of a single paramagnetic molecule containing a gadolinium (Gd^{3+}) ion. We confirm single-molecule resolution using optical fluorescence and atomic force microscopy to colocalize one NV center and one Gd^{3+}-containing molecule. Possible applications include nanoscale and in vivo magnetic spectroscopy and imaging of individual molecules.



KEYWORDS: *Nitrogen vacancy center, diamond, single-molecule spin, magnetometry, all-optical*

Precision magnetic sensing is essential to a wide array of technologies such as magnetic resonance imaging (MRI) with important applications in both the physical and life sciences. In particular, in biology and medicine functional magnetic resonance imaging (fMRI) has emerged as a primary workhorse for obtaining key physiological and pathological information noninvasively, such as blood and tissue oxygen level and redox status.[1−3] Developing nanoscale magnetic sensing applicable to individual molecules could enable revolutionary advances in the physical, biological, and medical sciences. Examples include determining the structure of single proteins and other biomolecules as well as in vivo measurements of small concentrations of reactive oxygen species that could lead to insights into cellular signaling, aging, mutations, and death.[4−7] The practical realization of these ideas is extremely challenging, however, as it requires sensitive detection of weak magnetic fields associated with individual electronic or nuclear spins at nanometer scale resolution, often under ambient, room-temperature conditions. Many state-of-the-art magnetic sensors, including superconducting quantum interference devices (SQUIDs),[8] semiconductor Hall effect sensors,[9] and spin exchange relaxation-free atomic magnetometers,[10] offer outstanding sensitivity, but their macroscopic nature precludes individual spin sensing. Sensing ensembles of paramagnetic molecules in biological and medical systems is currently performed using bulk electron spin resonance (ESR), which has a detection limit of roughly 10^7 electron-spins.[11] Magnetic resonance force microscopy has been used to detect individual electronic spins but at cryogenic, milliKelvin temperature.[12,13]

The nitrogen-vacancy (NV) center in diamond is a promising precision magnetic field sensor with nanoscale resolution.[14−17] Ensembles of NV centers in bulk diamond have been used to sense paramagnetic molecules in solution[18] with sensitivity of $\sim 10^3$ statistically polarized spins and spatial resolution of approximately 450 nm; NV centers in nanodiamonds have been used to sense paramagnetic ions covering the nanodiamond surface[19] and in a lipid bilayer formed around the nanodiamond surface.[20] Shallow NV centers have also been used to detect small ensembles of nuclear spins in samples covering the surface of a bulk diamond crystal.[21,22] In this work, we covalently attach target molecules to the diamond surface and demonstrate nanoscale localization and magnetic sensing of individual

Received: August 4, 2014
Revised: October 10, 2014
Published: October 21, 2014

 © 2014 American Chemical Society dx.doi.org/10.1021/nl502988n | *Nano Lett.* 2014, 14, 6443−6448

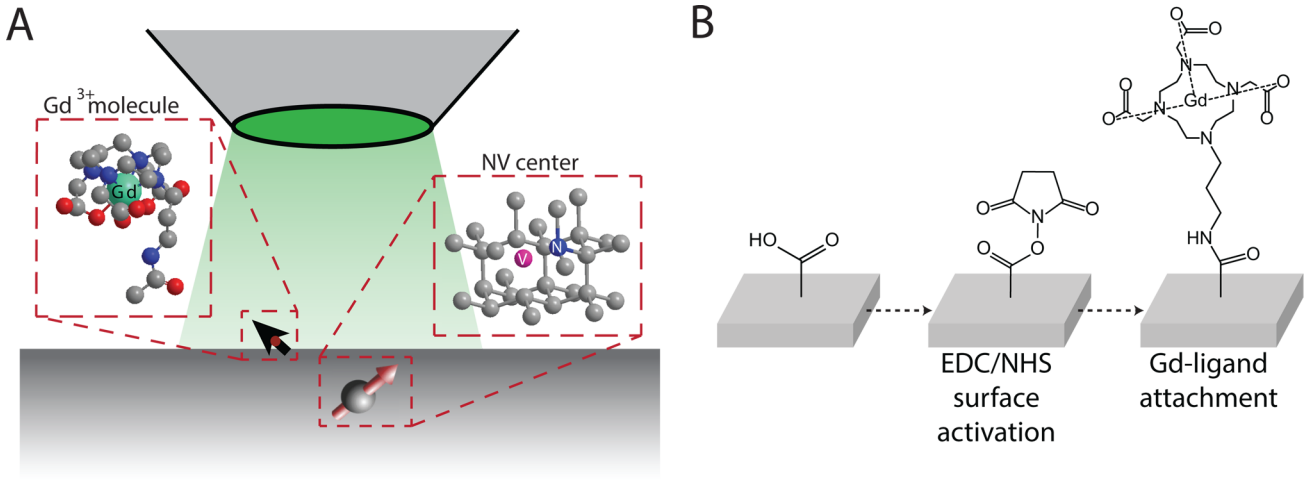


Figure 1. Schematic of measurement setup and sample preparation. (A) Single-molecule electron spin detection using a single shallow NV center in bulk diamond. Gd^{3+} molecules are attached to the surface of a bulk diamond crystal with widely separated NV centers located at a nominal depth of 6 nm below the diamond surface. NV center optical pumping and fluorescence detection is performed using a confocal microscope (objective shown). (B) Chemical procedure for attaching Gd^{3+} molecules to the diamond surface. EDC and NHS are used to activate carboxyl groups on the diamond surface so that they react readily with Gd^{3+} molecules functionalized with amine groups.

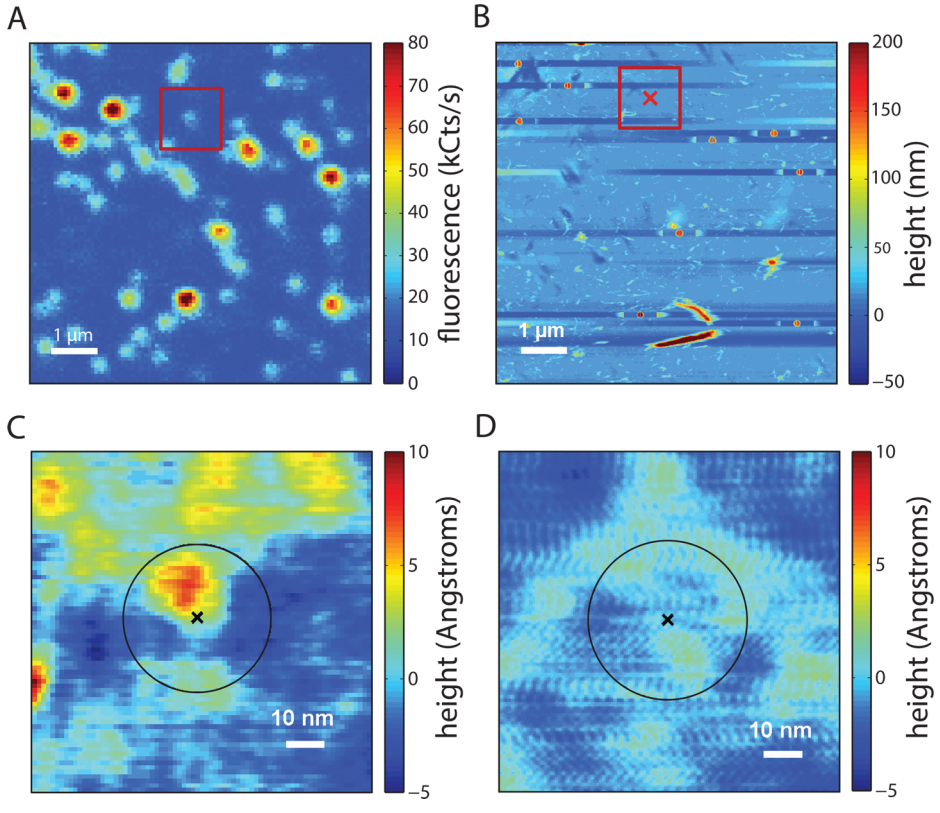


Figure 2. Co-localization of a single shallow NV center and a Gd^{3+} molecule. (A) Fluorescence image of a 7.5 μm × 7.5 μm area of the diamond crystal, showing several gold nanoparticles (bright spots), and NV centers (less intense spots). Location of a single NV center, marked by a red square, was determined in relation to the gold nanoparticles. (B) AFM image of the same region of the diamond surface, showing gold nanoparticles (red dots). The red cross marks the location of the NV center, deduced from the fluorescence image. (C) AFM image of the 100 nm × 100 nm region of the diamond surface centered at the location of the NV center (marked by a black cross). The black circle shows the one standard deviation uncertainty in the NV center position with a single Gd^{3+} molecule present within the circle (bright spot). (D) AFM image of the same area as in (C) after Gd^{3+} molecules were removed from the diamond surface.

nonfluorescent paramagnetic molecules. This represents an important step toward the development of nanoscale magnetic imaging of biomolecules under ambient conditions.

In our approach, the target molecules are covalently attached to the diamond surface, and magnetic sensing of these molecules is performed under ambient conditions using a single shallow NV center as an all-optical nanoscale magnetometer (Figure 1A). Importantly, the shallow NV center is close enough to the surface that it can detect the fluctuating magnetic field produced by the electronic spin of a single paramagnetic molecule, while

dx.doi.org/10.1021/nl502988n | *Nano Lett.* 2014, 14, 6443−6448

maintaining good NV center spin coherence and optical properties. We apply this technique to detect a single paramagnetic molecule composed of a gadolinium ion (Gd^{3+}) chelated by an amine-terminated organic ligand (abbreviated as Gd^{3+} molecule below). Single-molecule sensing is confirmed by identifying NV centers that have only a single target molecule within the sensing area on the diamond surface.

Our scheme for covalently attaching molecules to the diamond surface relies on the coupling of the amine-functionalized Gd^{3+} molecule to the carboxylic group on the diamond surface: in order to improve this coupling efficiency, we activated the surface carboxylic group using a water-soluble mixture of 1-ethyl-3-(3-(dimethylamino)propyl)carbodiimide (EDC) and *N*-hydroxysulfosuccinimide (NHS) (Figure 1B). This method yielded uniform surface coverage of molecules with little clumping (see Supporting Information), and the surface density of molecules could be controlled by varying the concentration of the Gd^{3+} molecules during the reaction. This procedure can be used to covalently attach any water-soluble amine-terminated molecule to the diamond surface with controlled surface coverage. Since covalent attachment utilizes diamond surface carboxylic groups, the resulting molecular surface density was always less than a monolayer.

In our experiments, we used atomic force microscopy (AFM) to quantify the surface density of these molecules and to identify their proximity to a given shallow NV center. AFM measurements show that a clean diamond surface exhibits atomically smooth regions of typically a few square micrometers. When the Gd^{3+} molecules were attached, we observed circular features with mean height of 8 Å in the AFM scans. The heights, radii, and density of these features were consistent with single Gd^{3+} molecules covalently attached to the diamond surface (molecular dimensions were estimated from bond lengths and angles, see Supporting Information). As an independent check of the surface molecule density, we added a single Cy3 dye molecule to each Gd^{3+} molecule and then attached the resulting molecule to the diamond surface using the same chemical procedure as before. We then performed surface fluorescence measurements to deduce the Cy3 surface density and compared the result to the density of the surface molecules measured using AFM. The results of these independent measurements were consistent with each other, providing strong evidence that the 8 Å-high AFM features are indeed single molecules (see Supporting Information).

In order to determine the proximity of Gd^{3+} molecules to a given shallow NV center with nanoscale precision, we performed a three-step colocalization experiment (Figure 2). First, we coated the diamond surface (via electrostatic attachment) with 100 nm diameter gold nanoparticles that fluoresce in the same spectral region as the NV centers and are optically resolvable individually. Second, we performed a fluorescence scan to determine the locations of individual NV centers and gold nanoparticles optically (Figure 2A). Finally, we performed AFM topography measurements to determine the locations of gold nanoparticles and Gd^{3+} molecules (Figure 2B). Because the nanoparticles appear in both optical and AFM images, we can use the locations of nanoparticles to combine the fluorescence and AFM measurements and deduce the lateral positions of Gd^{3+} molecules relative to an NV center with uncertainty of approximately 15 nm (see Supporting Information). Figure 2C shows an example of this colocalization experiment: an AFM image of Gd^{3+} molecules together with the position of a single shallow NV center, marked by a cross (the circle shows the NV center position uncertainty at one standard deviation). When the Gd^{3+} molecules were removed from the diamond surface, the AFM scan of the same region showed the absence of 8 Å-high features, confirming the successful removal of molecules (Figure 2D).

Once we located a single Gd^{3+} molecule with a nearby NV center, we performed all-optical magnetic sensing of this molecule. At room temperature, the $S = 7/2$ electron spin of the Gd^{3+} ion fluctuates with a relaxation rate (γ_{Gd}) on the order of 10 GHz.[23,24] These spin-flips give rise to a fluctuating magnetic field at the location of the NV center with a Fourier spectrum of width $\approx \gamma_{Gd}$. The Fourier component of this fluctuating magnetic field at the frequency corresponding to the zero-field splitting of the NV center ground state spin manifold ($S = 1$) drives magnetic dipole transitions between these sublevels (Figure 3A). We detected these transitions by first optically pumping the NV center into the $m_s = 0$ sublevel and then measuring its spin-state-dependent fluorescence after a variable delay time τ (Figure 3B,

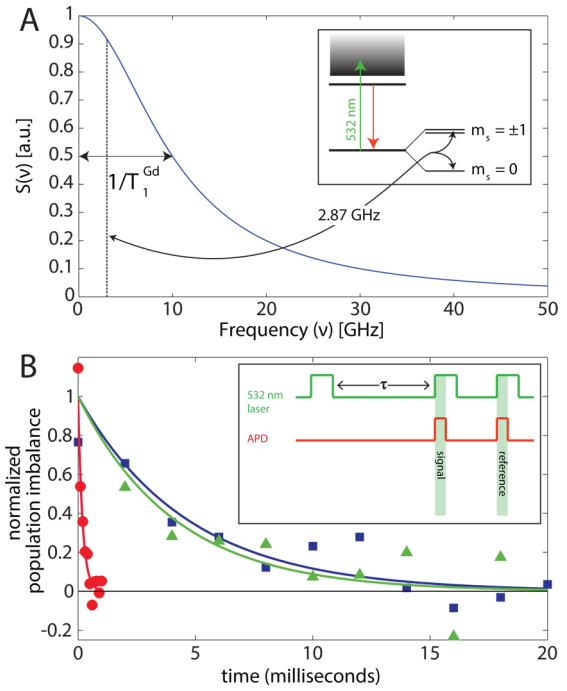


Figure 3. Measurement of magnetic noise from a single Gd^{3+} molecule attached to a diamond surface using a single shallow NV center. (A) Schematic power spectrum of the fluctuating magnetic field due to relaxation of the Gd^{3+} electronic spin (inset: NV-center electronic excited and ground states, with ground-state spin sublevels). Fourier components of this spectrum near the frequency resonant with the NV center zero-magnetic-field splitting lead to an increase in the NV center spin-state population relaxation rate. (B) Demonstration of NV magnetic sensing of a single Gd^{3+} molecule on the surface of bulk diamond. Measurements of the NV center spin-state population difference relaxation and exponential fits. Clean diamond surface: blue squares and blue line. Gd^{3+} molecules attached to the diamond surface: red circles and red line. Recleaned diamond surface: green triangles and green line. The AFM image for this NV center is shown in Figure 2C, where it is demonstrated that it is in proximity to a single Gd^{3+} molecule. The scatter of the experimental data points is consistent with photon shot noise with total averaging time on the order of an hour (not including the time needed to correct for setup drifts). Inset: Pulse measurement scheme for measuring the NV center spin-state relaxation rate. An avalanche photodiode (APD) was used for NV-center red fluorescence detection.

dx.doi.org/10.1021/nl502988n | *Nano Lett.* 2014, 14, 6443−6448

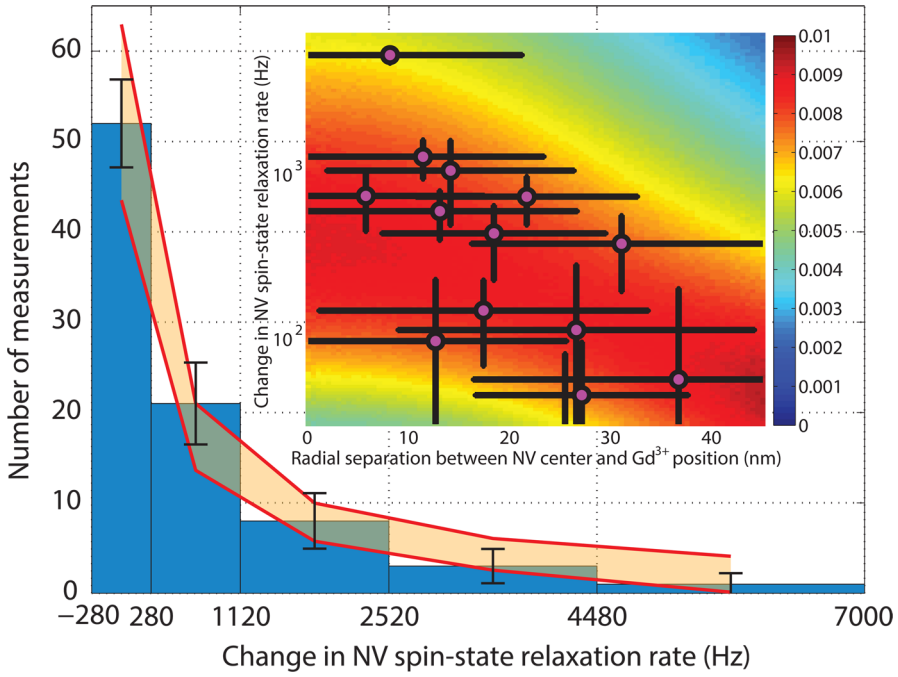


Figure 4. Magnetic noise measurements in the single Gd^{3+} molecule sensing regime. Results of 85 Gd-induced NV center spin-state relaxation rate measurements, along with a Monte Carlo simulation band. The experimental data are grouped into five bins with the error bars calculated by combining bin sampling uncertainty and relaxation rate fitting uncertainty (see Supporting Information). The theoretical band was obtained from Monte Carlo simulations of the experiment with parameters given in the text. Inset: results of 14 colocalization and NV center spin-state relaxation rate measurements in which a single Gd^{3+} molecule was identified near a single shallow NV center. The background displays the results of Monte Carlo simulations of the experiment with the color scale indicating the probability density of obtaining a particular NV center spin-state relaxation rate for a given separation between the NV center and the proximal Gd^{3+} molecule. The simulation was performed for 20 nm separation between Gd^{3+} molecules, and NV center colocalization uncertainty of 15 nm. For a quantitative comparison, we performed a two-variable Kolmogorov−Smirnov statistical test, resulting in the Z-statistic value of 1.1, which indicates that the data points are consistent with the simulated distribution (see Supporting Information).

inset). In the absence of Gd^{3+} molecules, the NV spin-state population difference decayed with rate $\Gamma_{intrinsic}$ due to spin−lattice relaxation. However, when the NV center was in proximity to a Gd^{3+} molecule, the measured NV population relaxation rate increased to $\Gamma_{total} = \Gamma_{intrinsic} + \Gamma_{induced}$ (see Supporting Information), which constitutes magnetic sensing of single-molecule electron spin. For example, the red circles in Figure 3B show the result of the NV spin-state relaxation measurements for the NV−Gd^{3+} molecule pair displayed in Figure 2C (the red line is an exponential fit); the blue squares in Figure 3B illustrate the spin-state relaxation rate of the same NV center prior to attachment of the Gd^{3+} molecule. The comparison of these measurements clearly shows a dramatic increase of the relaxation rate in the presence of a single Gd^{3+} molecule. Once the molecule was removed (Figure 2D), the relaxation returned to the intrinsic rate (green triangles in Figure 3B).

The inset of Figure 4 summarizes the measured Gd-induced relaxation rates of for multiple NV−Gd^{3+} molecule pairs with varying NV-molecule separations. We performed a total of 23 colocalization experiments, together with population relaxation measurements of the corresponding NV centers. In 14 of the 23 colocalization experiments, we could reliably identify single Gd^{3+} molecules and extract the separation between an NV center and a Gd^{3+} molecule; while in the remaining 9 experiments, we could not do so because of finite AFM tip resolution or rough surface topography. Seven of the data points exhibit a significant (greater than two standard deviation) increase in NV spin relaxation, and the corresponding colocalization measurements show the presence of a single Gd^{3+} molecule near the NV center position. As noted above, removal of the Gd^{3+} molecules from the diamond surface resulted in the relaxation rate returning to its intrinsic value in all cases.

A comparison of these data with Monte Carlo simulations (shown as background color plot in the inset of Figure 4) provides further evidence of NV magnetic detection of a single-molecule electron spin. In the simulation, we calculated the probability density of obtaining a particular NV spin relaxation rate for a given NV−Gd^{3+} molecule separation (see Supporting Information) within experimental uncertainties. We used an NV center depth of 6 nm, derived from calculations for 3 keV nitrogen ion implantation energy, a mean Gd^{3+} molecule spacing of 20 nm, derived from the AFM and Cy3 measurements described above, and a Gd^{3+} spin-relaxation rate of 10 GHz.[23,24] As seen in the inset of Figure 4, the experimental data points are consistent with the simulated probabilities (see Supporting Information).

Additional evidence for magnetic detection of single-molecule electron spins is provided by an independent set of 85 spin relaxation rate measurements that we performed on 26 shallow NV-centers over several cycles of Gd^{3+} molecule attachment and removal. As shown in the main plot of Figure 4, the resulting data are grouped into five bins with the error bars calculated by combining the bin sampling and relaxation rate fitting uncertainties (see Supporting Information). Also shown in this figure is a band of theoretically calculated NV spin relaxation rates, which we obtained from Monte Carlo simulations of the experiment, with the NV center depth of 6 nm, Gd^{3+} spin-flip rate varying in the range of 10 to 20 GHz, and mean Gd^{3+} surface density varying in the range of $1/(20\ nm)^2$ to $1/(25\ nm)^2$. These parameters yield simulated NV-center spin relaxation rate

dx.doi.org/10.1021/nl502988n | Nano Lett. 2014, 14, 6443−6448

distributions that are consistent with experimental data, again confirming that the observed NV spin relaxation rate increase is due to the proximity of a single-molecule electron spin. While other sets of model parameters in principle can be fit to the experimental data, all realistic model fit parameters correspond to regimes in which only a single Gd^{3+} spin contributes to increased NV center spin-state relaxation rate (see Supporting Information). The "sensing radius" of an NV-center (defined as the NV−Gd^{3+} molecule separation for which the change in NV-center spin relaxation rate is equal to the measurement uncertainty) is determined to be approximately 12 nm. This means that with probability over 80% only a single Gd^{3+} molecule can substantially contribute to the induced NV-center spin relaxation rate even for highest Gd^{3+} molecule densities used.

The detection sensitivity of our experiment is limited by photon shot noise. By monitoring NV-center fluorescence after optical pumping and a relaxation-in-the-dark period of ∼2 ms, chosen to be on the order of the NV-center intrinsic T_1 time, a single Gd^{3+} molecule spin at a distance of 10 nm can be detected after approximately 5 min of averaging (see Supporting Information). The sensitivity to other paramagnetic species depends on their magnetic moments and the magnitude of their fluctuating magnetic fields at the frequency corresponding to the $m_s = 0 \rightarrow m_s = \pm 1$ transition (see Supporting Information), which can be varied by applying a constant magnetic field. In order to detect radicals with long relaxation times, such as some nitroxides, NV spin coherence relaxation (affecting the measured T_2 time) may be most suitable.[25]

Our method for all-optical magnetic sensing of single paramagnetic molecules using shallow NV centers in diamond has potential implications to studies of a wide range of biochemical molecules and processes. Together with recent experiments demonstrating NV magnetic sensing of nanoscale ensembles of nuclear spins,[21,22] the combination of single-molecule covalent attachment, colocalization, and magnetic sensing techniques is an important step toward magnetic imaging measurements on individual biological molecules attached to the diamond surface.[26] Our magnetic measurement scheme directly detects the magnetic field created by a paramagnetic molecule without the need for fluorescent tagging and can be applied to detect and study small molecules without suffering from blinking or photobleaching.[27] Since NV center-based magnetometry was recently shown to be biocompatible,[28] our approach can also be used for in vivo magnetic sensing with single-molecule sensitivity. Specifically, our covalent attachment scheme can be extended to nanodiamonds, functionalizing them to target certain cellular organelles, as well as functionalizing with chemical species (spin traps) that react with short-lived free radicals to produce persistent paramagnetic molecules, which can then be magnetically detected. Because radicals are thought to play a key role in biochemical processes such as cellular signaling, aging, mutations, and death,[4−7] the ability to detect small concentrations (approaching 100 μM, corresponding to mean separation of approximately 25 nm) of short-lived radicals inside living cells could be a powerful tool in studying these processes with possible applications for disease detection and drug development. Finally, our methods could also find applications in nanoscale and materials science, for example, in studies of molecular magnets on a diamond surface, and when combined with the recently demonstrated scanning probe techniques[29] they could enable imaging of rapidly fluctuating magnetic fields near the surfaces of materials such as superconductors,[30] topological insulators,[8,31] and others (ferromagnets, multiferroics, and so forth).

■ ASSOCIATED CONTENT

Supporting Information

A detailed description of the experimental setup, sample preparation, AFM experiments and data analysis, simulations, and control experiments with La^{3+}. This material is available free of charge via the Internet at http://pubs.acs.org.

■ AUTHOR INFORMATION

Corresponding Authors

*E-mail: (H.P.) Hongkun_Park@harvard.edu.
*E-mail: (M.D.L) lukin@physics.harvard.edu.

Author Contributions

¶A.O.S., N.C., I.L. contributed equally to this work.

Notes

The authors declare no competing financial interest.

■ ACKNOWLEDGMENTS

We acknowledge Eric Bersin, Yiwen Chu, Mike Grinolds, Nathalie de Leon, Brendan Shields, Joshua Vaughan, Amir Yacoby, and Norman Yao for experimental help and fruitful discussions. This work was supported by the Defense Advanced Research Projects Agency (QuASAR program), NSF, CUA, ARO MURI, Element Six Inc, Packard Foundation, NSERC (NC) and NDSEG (IL). The authors declare no competing financial interest.

■ REFERENCES

(1) Logothetis, N. K. *Nature* **2008**, *453*, 869−878.
(2) Matsumoto, K.-i.; Subramanian, S.; Murugesan, R.; Mitchell, J. B.; Krishna, M. C. *Antioxid. Redox Signaling* **2007**, *9*, 1125−1141.
(3) Ahrens, E. T.; Bulte, J. W. M. *Nat. Rev. Immunol.* **2013**, *13*, 755−763.
(4) Netzer, N.; Goodenbour, J. M.; David, A.; Dittmar, K. A.; Jones, R. B.; Schneider, J. R.; Boone, D.; Eves, E. M.; Rosner, M. R.; Gibbs, J. S.; et al. *Nature* **2009**, *462*, 522−526.
(5) Halliwell, B. *Biochem. J.* **2007**, *401*, 1−11.
(6) Valko, M.; Leibfritz, D.; Moncol, J.; Cronin, M. T.; Mazur, M.; Telser, J. *Int. J. Biochem. Cell Biol.* **2007**, *39*, 44−84.
(7) James, S. J.; Cutler, P.; Melnyk, S.; Jernigan, S.; Janak, L.; Gaylor, D. W.; Neubrander, J. A. *Am. J. Clin. Nutr.* **2004**, *80*, 1611−1617.
(8) Nowack, K. C.; Spanton, E. M.; Baenninger, M.; König, M.; Kirtley, J. R.; Kalisky, B.; Ames, C.; Leubner, P.; Brüne, C.; Buhmann, H.; et al. *Nat. Mater.* **2013**, *12*, 787−791.
(9) Bending, S. J. *Adv. Phys.* **1999**, *48*, 449−535.
(10) Allred, J.; Lyman, R.; Kornack, T.; Romalis, M. *Phys. Rev. Lett.* **2002**, *89*, 130801.
(11) Blank, A.; Dunnam, C. R.; Borbat, P. P.; Freed, J. H. *Appl. Phys. Lett.* **2004**, *85*, 5430.
(12) Rugar, D.; Budakian, R.; Mamin, H. J.; Chui, B. W. *Nature* **2004**, *430*, 329−332.
(13) Degen, C. L.; Poggio, M.; Mamin, H. J.; Rettner, C. T.; Rugar, D. *Proc. Natl. Acad. Sci. U.S.A.* **2009**, *106*, 1313−1317.
(14) Taylor, J. M.; Cappellaro, P.; Childress, L.; Jiang, L.; Budker, D.; Hemmer, P. R.; Yacoby, A.; Walsworth, R.; Lukin, M. D. *Nat. Phys.* **2008**, *4*, 810−816.
(15) Maze, J. R.; Stanwix, P. L.; Hodges, J. S.; Hong, S.; Taylor, J. M.; Cappellaro, P.; Jiang, L.; Dutt, M. V. G.; Togan, E.; Zibrov, A. S.; et al. *Nature* **2008**, *455*, 644−647.
(16) Balasubramanian, G.; Chan, I. Y.; Kolesov, R.; Al-Hmoud, M.; Tisler, J.; Shin, C.; Kim, C.; Wojcik, A.; Hemmer, P. R.; Krueger, A.; et al. *Nature* **2008**, *455*, 648−651.

(17) Hall, L. T.; Hill, C. D.; Cole, J. H.; Städler, B.; Caruso, F.; Mulvaney, P.; Wrachtrup, J.; Hollenberg, L. C. L. *Proc. Natl. Acad. Sci. U.S.A.* **2010**, *107*, 18777.
(18) Steinert, S.; Ziem, F.; Hall, L. T.; Zappe, A.; Schweikert, M.; Götz, N.; Aird, A.; Balasubramanian, G.; Hollenberg, L.; Wrachtrup, J. *Nat. Commun.* **2013**, *4*, 1607.
(19) Tetienne, J.-P.; Hingant, T.; Rondin, L.; Cavaillès, A.; Mayer, L.; Dantelle, G.; Gacoin, T.; Wrachtrup, J.; Roch, J.-F.; Jacques, V. *Phys. Rev. B* **2013**, *87*, 235436.
(20) Kaufmann, S.; Simpson, D. A.; Hall, L. T.; Perunicic, V.; Senn, P.; Steinert, S.; McGuinness, L. P.; Johnson, B. C.; Ohshima, T.; Caruso, F.; et al. *Proc. Natl. Acad. Sci. U.S.A.* **2013**, *110*, 10894.
(21) Staudacher, T.; Shi, F.; Pezzagna, S.; Meijer, J.; Du, J.; Meriles, C. A.; Reinhard, F.; Wrachtrup, J. *Science* **2013**, *339*, 561−563.
(22) Mamin, H. J.; Kim, M.; Sherwood, M. H.; Rettner, C. T.; Ohno, K.; Awschalom, D. D.; Rugar, D. *Science* **2013**, *339*, 557−560.
(23) Bierig, R.; Weber, M.; Warshaw, S. *Phys. Rev.* **1964**, *134*, A1504−A1516.
(24) Kim, H. K.; Lee, G. H.; Kim, T. J.; Chang, Y. *Bull. Korean Chem. Soc.* **2009**, *30*, 849.
(25) Hall, L.; Hill, C.; Cole, J.; Hollenberg, L. *Phys. Rev. B* **2010**, *82*, 045208.
(26) Perunicic, V. S.; Hall, L. T.; Simpson, D. A.; Hill, C. D.; Hollenberg, L. C. L. 2013, ArXiv: 1307.8220.
(27) Giepmans, B. N. G.; Adams, S. R.; Ellisman, M. H.; Tsien, R. Y. *Science* **2006**, *312*, 217−224.
(28) Le Sage, D.; Arai, K.; Glenn, D. R.; DeVience, S. J.; Pham, L. M.; Rahn-Lee, L.; Lukin, M. D.; Yacoby, A.; Komeili, A.; Walsworth, R. L. *Nature* **2013**, *496*, 486−489.
(29) Grinolds, M. S.; Hong, S.; Maletinsky, P.; Luan, L.; Lukin, M. D.; Walsworth, R. L.; Yacoby, A. *Nat. Phys.* **2013**, *9*, 215−219.
(30) Kirtley, J. R. *Rep. Prog. Phys.* **2010**, *73*, 126501.
(31) Zhang, H.; Liu, C.-X.; Qi, X.-L.; Dai, X.; Fang, Z.; Zhang, S.-C. *Nat. Phys.* **2009**, *5*, 438−442.